A direct traction boundary integral equation method for three-dimension crack problems in infinite and finite domains

Guizhong Xie, Jianming Zhang*, Cheng Huang, Chenjun Lu, Guangyao Li

State Key Laboratory of Advanced Design and Manufacturing for Vehicle Body, College of Mechanical and Vehicle Engineering, Hunan University, Changsha 410082, China

Correspondence to: Jianming Zhang
College of Mechanical and Vehicle Engineering, Hunan University, Changsha 410082, China
Telephone: +86-731-88823061
E-mail: zhangjm@hnu.edu.cn

Abstract

This paper presents a direct traction boundary integral equation method (TBIEM) for three-dimensional crack problems. The TBIEM is based on the traction boundary integral equation (TBIE). The TBIE is collocated on both the external boundary and one of the crack surfaces. The displacements and tractions are used as unknowns on the external boundary and the relative crack opening displacements (CODs) are introduced as unknowns on the crack surface. In our implementation, all the surfaces of the considered structure are discretized into discontinuous elements to satisfy the continuity requirement for the existence of finite-part integrals, and special crack-front elements are constructed to capture the crack-tip behavior. To calculate the finite-part integrals, an adaptive singular integral technique is proposed. The stress intensity factors (SIFs) are computed through a modified COD extrapolation method. Numerical examples of SIFs computation are presented to demonstrate the accuracy and efficiency of our method.

Keywords: traction boundary integral equation, discontinuous elements, singular integrals, cracks opening displacement, stress intensity factor.

1. Introduction

SIFs play an important role in characterizing fracture behavior in linear elastic fracture mechanics. Accurate evaluation of SIFs has challenged many numerical modeling techniques. The boundary element method (BEM) is an attractive method for the calculation of SIFs (Cruse, 1988; Aliabadi, 1997). However, the conventional

BEM encounters considerable difficulties for crack problems because a singular system of equations is always obtained (Cruse, 1988; Aliabadi, 1997). To circumvent the difficulties, various methods (Pan, 1997) within the scope of BEM including the special Green's method (Telles, 1995), the multi-domain techniques (Blandford et al., 1981), the displacement discontinuity or dislocation method (Crouch, 1983; Pan, 1991), the Galerkin symmetric method (Sirtori et al., 1992) and the dual boundary integral equations method (DBIE) (Mi and Aliabadi 1992; Chen and Chen, 1995; Cisilino and Aliabadi, 1999; Wilde, 1999; Pan, 2000; Wang and Yao, 2006) have been proposed. Among the above methods, DBIEM is a promising method (Pan, 1997; Pan, 2000). However, the DBIEM formulation is based on a pair of boundary integral equations, namely, the displacement and traction boundary integral equations. In the numerical implementation of DBIEM, four types of singular integrals are involved in the two boundary integral equations. Special singular integrals techniques are required for the singular integrals. In the standard DBIEM, the weakly singular integrals are computed by variable transformations (Lachat and Watson, 1976). And the strongly singular integrals which are involved in the displacement integral equation are calculated directly by the rigid-body motion method. While the strongly singular and hypersingular integrals associated with the traction integral equation are evaluated by the singular subtraction technique (Aliabadi et al, 1985; Mi and Aliabadi, 1992; Guiggiani, 1998). The various methods for different type singular integrals can not be unified into a uniform formation. It is not easy for program code writing. So it is time to develop a new method which can overcome the trouble and which also inherits the advantage of the DBIEM.

In this paper, a direct TBIEM for three-dimensional crack problems in infinite and finite domains is proposed. The TBIEM formulation is based on the traction boundary integral equation (TBIE). The TBIE is collocated on both the external boundary and one of the crack surfaces. The displacements and tractions are used as unknown variables on the external boundary and the relative crack opening displacements (CODs) are introduced as unknowns on the crack surfaces. Only TBIE is required in this formulation and this formulation has the advantage resulting in a smaller system

of algebraic equations since only one of the crack surfaces needs to be discretized. In our implementation, in order to satisfy the continuity requirement for the existence of finite-part integrals, all the surfaces of the considered structure are discretized into 9-node discontinuous quadrilateral elements. To calculate the finite-part integrals more accurately, an adaptive element subdivision technique is adopted to improve the conventional singular subtraction technique. In the adaptive subdivision technique, the singular element is subdivided into several triangular and quadrangular patches. The integrals over each quadrangular patch are treated as nearly singular integrals, while the integrals over each triangular patch are computed by the singular subtraction technique based on a Taylor series expansion of kernel function, shape functions, and the transformation Jacobian. Special crack-front elements considering the position of the crack fronts are employed. The special crack-front elements successfully model the distribution of displacements in the vicinity of the crack tips. With the help of the adaptive singular integral technique and specially constructed elements, the SIFs along the crack-front are computed through a modified COD extrapolation method.

The outline of this paper is as follows. In section 2, we introduce the TBIEM formulation. Section 3 introduces the modeling strategy. In section 4, the treatment of the singular integrals is described. The method for the calculation of SIFs is given in Section 5. Numerical examples are shown in Section 6. The paper ends with conclusions in Section 7.

2. The traction boundary integral equation method formulation

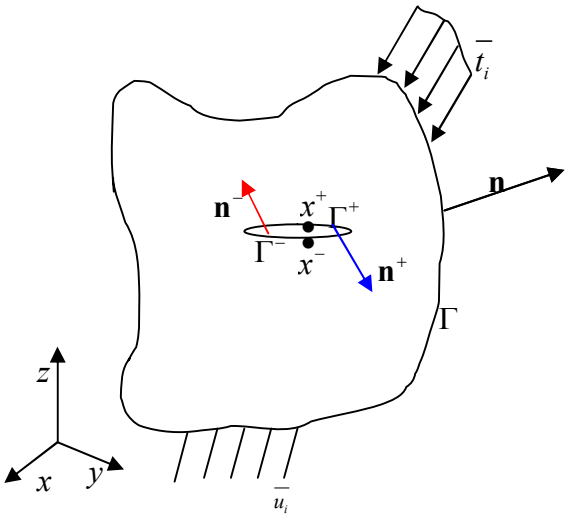

Fig. 1. A finite body with a crack

As shown in Fig. 1, a finite body with a crack is considered. Γ is the external boundary. Γ^+ is the upper crack surface, while Γ^- is the lower crack surface. The traction at y can be represented by

$$\frac{1}{2}t_j(y) = n_i(y)\int_{\Gamma+\Gamma^+ +\Gamma^-} U^*_{ijk}(x,y)t_k(x)dS(x) - n_i(y)\int_{\Gamma+\Gamma^+ +\Gamma^-} T^*_{ijk}(x,y)u_k(x)dS(x) \tag{1}$$

where $y=(y_1,y_2,y_3)$ is the source point and $x=(x_1,x_2,x_3)$ is the field point. $U^*_{ijk}(x,y)$ and $T^*_{ijk}(x,y)$ contain several derivatives of the Kelvin fundamental solutions, together with the elastic constants. Expressions for $U^*_{ijk}(x,y)$ and $T^*_{ijk}(x,y)$ are:

$$U^*_{ijk}(P_S,Q) = \frac{3r_{,i}r_{,j}r_{,k} + (1-2\mu)(r_{,i}\delta_{jk} + r_{,j}\delta_{ik} - r_{,k}\delta_{ij})}{8\pi(1-\mu)r^2} \tag{2}$$

$$\begin{aligned} T^*_{ijk}(P_S,Q) = {} & \frac{G}{4\pi(1-\mu)r^3}\{(1-2\mu)(\delta_{ik}n_j + \delta_{kj}n_i + 3r_{,j}r_{,i}n_{,k}) - (1-4\mu)\delta_{ij}n_k \\ & + 3\mu r_{,k}(r_{,i}n_j + r_{,j}n_i) + 3\frac{\partial r}{\partial n}[(1-2\mu)\delta_{ij}r_{,k} + \mu(\delta_{ik}r_{,j} + \delta_{jk}r_{,i}) - 5r_{,i}r_{,k}r_{,j}]\} \end{aligned} \tag{3}$$

where r is the distance between x and y; G, μ and δ_{ij} represent the shear modulus, Poisson's ratio and the Kronecker delta, respectively; n denotes the unit outward normal vector at the point x on the boundary. $n(y)=(n_1(y),n_2(y),n_3(y))$ denotes the unit outward normal vector at the point y, and $r_{,i}=\partial r/\partial x_i$, $r_{,j}=\partial r/\partial x_j$.

From the properties of Kelvin's fundamental solutions and the traction equilibrium is assumed on the crack surfaces, we have

$$t_k(x^+) = -t_k(x^-),\ U^*_{ijk}(x^+,y) = U^*_{ijk}(x^-,y),\ T^*_{ijk}(x^+,y) = -T^*_{ijk}(x^-,y) \tag{4}$$

where $x^+\in\Gamma^+, x^-\in\Gamma^-$, $t_k(x^+)$ is the traction on the upper crack surface, while $t_k(x^-)$ is the traction on the lower crack surface.

We assume y is on the external boundary, using Eq. (4), the following equations can be obtained:

$$\int_{\Gamma+\Gamma^+ +\Gamma^-} U_{ijk}^*(x,y)t_k(x)dS(x)=\int_{\Gamma} U_{ijk}^*(x,y)t_k(x)dS(x) \tag{5}$$

$$\begin{aligned}&\int_{\Gamma+\Gamma^+ +\Gamma^-} T_{ijk}^*(x,y)u_k(x)dS(x)=\\&\int_{\Gamma} T_{ijk}^*(x,y)u_k(x)dS(x)+\int_{\Gamma^+} T_{ijk}^*(x,y)u_k^+(x)dS(x)+\int_{\Gamma^-} T_{ijk}^*(x,y)u_k^-(x)dS(x)\\&=\int_{\Gamma} T_{ijk}^*(x,y)u_k(x)dS(x)+\int_{\Gamma^+} T_{ijk}^*(x,y)\Delta u_k(x)dS(x)\end{aligned} \tag{6}$$

where $u_k^+(x)$ is the displacement on the upper crack surface, while $u_k^-(x)$ is the displacement on the lower crack surface. $\Delta u_k(x)=u_k^+(x)-u_k^-(x)$.

Substituting Eq. (5) and Eq. (6) into Eq. (1), Eq. (1) can be written as:

$$\begin{aligned}&\frac{1}{2}t_j(y)=n_i(y)\int_{\Gamma} U_{ijk}^*(x,y)t_k(x)dS(x)-n_i(y)\int_{\Gamma} T_{ijk}^*(x,y)u_k(x)dS(x)\\&-n_i(y)\int_{\Gamma^+} T_{ijk}^*(x,y)\Delta u_k(x)dS(x), \qquad y\in\Gamma\end{aligned} \tag{7}$$

We assume y is on the upper crack surfaces, Eq. (1) should be written as:

$$\begin{aligned}&\frac{1}{2}\left\{t_j(y^+)-t_j(y^-)\right\}=n_i(y^+)\int_{\Gamma+\Gamma^+ +\Gamma^-} U_{ijk}^*(x,y)t_k(x)dS(x)\\&-n_i(y^+)\int_{\Gamma+\Gamma^+ +\Gamma^-} T_{ijk}^*(x,y)u_k(x)dS(x)\end{aligned} \tag{8}$$

Using Eq. (4), Eq. (8) can be simplified to:

$$\begin{aligned}&t_j(y^+)=n_i(y^+)\int_{\Gamma} U_{ijk}^*(x,y^+)t_k(x)dS(x)-n_i(y^+)\int_{\Gamma} T_{ijk}^*(x,y^+)u_k(x)dS(x)\\&-n_i(y^+)\int_{\Gamma^+} T_{ijk}^*(x,y^+)\Delta u_k(x)dS(x)\end{aligned} \tag{9}$$

Eqs. (7) and (9) constitute the new expressions for the TBIEM. It should be noted that in Eqs. (7) and (9), only the coefficients of $t_j(y)$ are different. So the singular integrals can be computed through a uniform singular subtraction method. Moreover, this new formulation has the advantage of resulting in a smaller system of algebraic equations since only one of the crack surfaces needs to be discretized. When this formulation is used for solutions of crack problems in infinite domains, Eq. (9) can be written as:

$$t_j(y^+)+n_i(y^+)\int_{\Gamma^+} T_{ijk}^*(x,y^+)\Delta u_k(x)dS(x)=0 \tag{10}$$

3. Modeling strategy

The use of the TBIE imposes certain restrictions on the choice of element to satisfy the continuity requirement for the existence of finite-part integrals (Mi and Aliabadi,

1992; Mi and Aliabadi, 1994).. Thus in our method, 9-node discontinuous quadrilateral Lagrangian elements (9DQLE) are employed for the uncracked boundary and crack surfaces while special crack-tip elements are used at the crack front. The 9-node discontinuous quadrilateral Lagrangian element is shown in Fig. 2(a). And the special crack-tip elements are shown in Fig. 2(b) and Fig. 2(c).

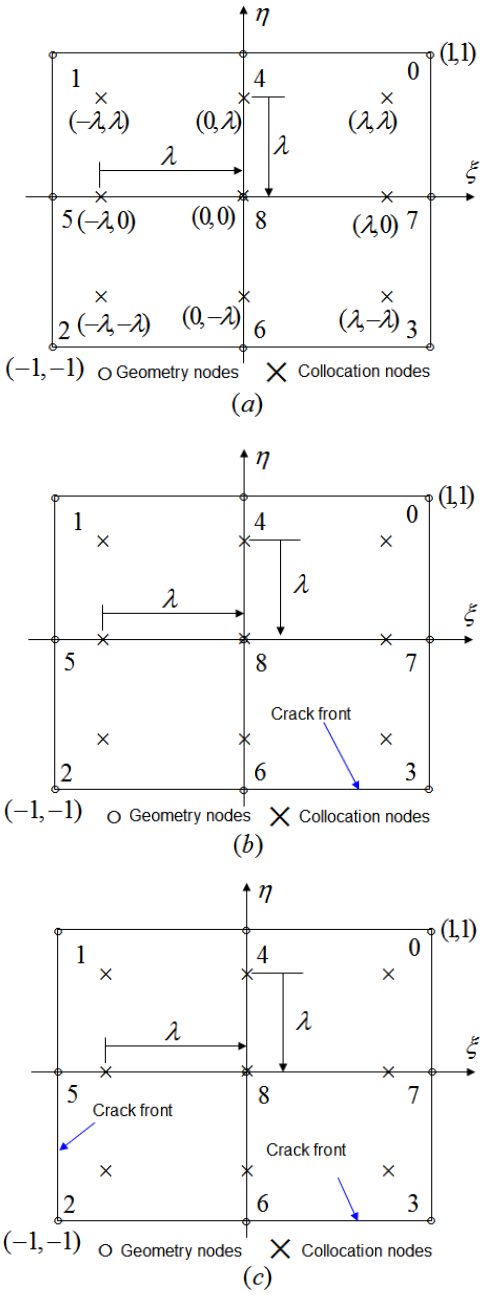

Fig. 2. Three types of elements

(a) 9-node discontinuous element (b) special crack-tip elements with one edge lying in the crack front (c) special crack-tip elements with two edges lying in the crack front

For elements of the three types, geometry and functionality are interpolated using

different sets of shape functions. Shape functions ϕ_{geo}^{i} used for the geometry are as follows:

$$\phi_{geo}^{0}=\frac{1}{4}\xi(1+\xi)(1+\eta)\eta$$
$$\phi_{geo}^{1}=-\frac{1}{4}\xi(1-\xi)(1+\eta)\eta$$
$$\phi_{geo}^{2}=\frac{1}{4}\xi(1-\xi)(1-\eta)\eta$$
$$\phi_{geo}^{3}=-\frac{1}{4}\xi(1+\xi)(1-\eta)\eta$$
$$\phi_{geo}^{4}=\frac{1}{2}(1+\xi)(1-\xi)(1+\eta)\eta$$
$$\phi_{geo}^{5}=-\frac{1}{2}\xi(1-\xi)(1+\eta)(1-\eta)$$
$$\phi_{geo}^{6}=-\frac{1}{2}(1+\xi)(1-\xi)(1-\eta)\eta$$
$$\phi_{geo}^{7}=\frac{1}{2}\xi(1+\xi)(1+\eta)(1-\eta)$$
$$\phi_{geo}^{8}=(1+\xi)(1-\xi)(1+\eta)(1-\eta) \tag{11}$$

The functional shape functions ϕ_{coll}^{i} for 9DQLE in Fig. 2(a) are as follows:

$$\phi_{Coll}^{0}=\frac{1}{4\lambda^{4}}\xi(\lambda+\xi)(\lambda+\eta)\eta$$
$$\phi_{Coll}^{1}=-\frac{1}{4\lambda^{4}}\xi(\lambda-\xi)(\lambda+\eta)\eta$$
$$\phi_{Coll}^{2}=\frac{1}{4\lambda^{4}}\xi(\lambda-\xi)(\lambda-\eta)\eta$$
$$\phi_{coll}^{3}=-\frac{1}{4\lambda^{4}}\xi(\lambda+\xi)(\lambda-\eta)\eta$$
$$\phi_{coll}^{4}=\frac{1}{2\lambda^{4}}(\lambda+\xi)(\lambda-\xi)(\lambda+\eta)\eta$$
$$\phi_{coll}^{5}=-\frac{1}{2\lambda^{4}}\xi(\lambda-\xi)(\lambda+\eta)(\lambda-\eta)$$
$$\phi_{coll}^{6}=-\frac{1}{2\lambda^{4}}(\lambda+\xi)(\lambda-\xi)(\lambda-\eta)\eta$$
$$\phi_{coll}^{7}=\frac{1}{2\lambda^{4}}\xi(\lambda+\xi)(\lambda+\eta)(\lambda-\eta)$$
$$\phi_{coll}^{8}=\frac{1}{\lambda^{4}}(\lambda+\xi)(\lambda-\xi)(\lambda+\eta)(\lambda-\eta) \tag{12}$$

The shape functions ϕ_{coll}^{i} for special crack tip elements are different from those of 9DQLE. Eight-node discontinuous elements with special shape functions have been

presented in Ref. (Mi and Aliabadi, 1994). In this work, 9-node discontinuous quadrilateral Lagrangian elements with special shape functions are proposed. Moreover, special crack tip elements with two edges lying in the crack fronts are also presented. And we will give a detailed deduction for the two types of special shape functions.

Let us assume that the crack front lies along the local coordinate $\eta = -1$, as shown in Fig. 2(b). Ref. (Mi and Aliabadi, 1994) indicated that the distance $r = |x(\xi,\eta) - x(\xi,-1)|$ is proportion to $\eta + 1$ in local coordinate system. The COD (Δu) over the element which is adjacent to the crack front can be written as:

$$\Delta u(\xi,\eta) = \Delta u^i M^i(\xi,\eta) = I_2(\xi) r^2 + I_1(\xi) r + I_0 \tag{13}$$

where $M^i(\xi,\eta)$ are discontinuous quadratic shape functions. To accurately model the COD as indicated in Ref. (Mi and Aliabadi, 1994), we should modified Eq. (13) into:

$$\begin{aligned} \Delta u(\xi,\eta) &= \overline{L_2}(\xi) r + \overline{L_1}(\xi)\sqrt{r} + \overline{L_0}(\xi) \\ &= L_2(\xi)(1+\eta) + L_1(\xi)\sqrt{(1+\eta)} + L_0(\xi) \end{aligned} \tag{14}$$

The shape functions should be of the form:

$$\begin{aligned} M^i &= a_1^i + a_2^i \xi + a_5^i \xi^2 + a_3^i \sqrt{1+\eta} + a_4^i \xi \sqrt{1+\eta} + a_7^i \xi^2 \sqrt{1+\eta} \\ &+ a_6^i (1+\eta) + a_8^i \xi (1+\eta) + a_9^i \xi^2 (1+\eta) \end{aligned} \tag{15}$$

where *i*=0,…8.

The shape functions in (15) must satisfy the conditions:

$$M^i(\xi_i,\eta_j) = \delta_{ij} \quad i=0,\ldots 8. \tag{16}$$

where δ_{ij} is the kronecker delta, and (ξ_i,η_i) are the functional coordinates for the discontinuous element in the (ξ,η) coordinate system, as illustrated in Fig. 2(a). Using Eq. (15), a set of 9×9 linear system of equations is obtained. Solving this system of equations by maple can yield the coefficients a_j^i. With $\lambda = 0.75$, the shape functions for the crack-tip element in Fig. 2(b) are obtained (APPENDIX A).

Let us assume that the crack fronts lie along the local coordinates $\xi = -1$ and

$\eta=-1$, as shown in Fig. 2(c). Using the same procedure, the shape functions should be of the form:

$$M^i = a_1^i + a_2^i\xi + a_5^i\eta + a_3^i\sqrt{1+\xi}\sqrt{1+\eta} + a_4^i\xi\sqrt{1+\xi}\sqrt{1+\eta} + a_7^i\eta\sqrt{1+\xi}\sqrt{1+\eta} + a_6^i(1+\xi)(1+\eta) + a_8^i\xi(1+\xi)(1+\eta) + a_9^i\eta(1+\xi)(1+\eta) \tag{17}$$

where *i*=0,…,8.

Using Eq. (17), a set of 9×9 linear system of equations is obtained. Solving this system of equations by maple will yield the coefficients a_j^i. With $\lambda=0.75$, the shape function for the crack-tip element Fig. 2(c) are obtained (APPENDIX B).

With the shape functions above, Eq. (7) and Eq. (9) can be written in a discretized form as:

$$\begin{aligned}
\frac{1}{2}t_j(y) &= n_i(y)\sum_{e=1}^{ne1}\left\{\sum_{\alpha=0}^{8}t_k^\alpha(x^a)\int_{\Gamma^e}U_{ijk}^*(x(\xi,\eta),y)N_\alpha(\xi,\eta)J(\xi,\eta)d\xi d\eta\right\} \\
&-n_i(y)\sum_{e=1}^{ne1}\left\{\sum_{\alpha=0}^{8}u_k^\alpha(x^a)\int_{\Gamma^e}T_{ijk}^*(x(\xi,\eta),y)N_\alpha(\xi,\eta)J(\xi,\eta)d\xi d\eta\right\} \\
&-n_i(y)\sum_{e=1}^{ne2}\left\{\sum_{\alpha=0}^{8}\Delta u_k^\alpha(x^a)\int_{\Gamma_e^+}T_{ijk}^*(x(\xi,\eta),y)N_\alpha(\xi,\eta)J(\xi,\eta)d\xi d\eta\right\} \qquad y\in\Gamma
\end{aligned} \tag{18}$$

$$\begin{aligned}
t_j(y^+) &= n_i(y^+)\sum_{e=1}^{ne1}\left\{\sum_{\alpha=0}^{8}t_k^\alpha(x^\alpha)\int_{\Gamma^e}U_{ijk}^*(x(\xi,\eta),y^+)N_\alpha(\xi,\eta)J(\xi,\eta)d\xi d\eta\right\} \\
&-n_i(y^+)\sum_{e=1}^{ne1}\left\{\sum_{\alpha=0}^{8}u_k^\alpha(x^\alpha)\int_{\Gamma^e}T_{ijk}^*(x(\xi,\eta),y^+)N_\alpha(\xi,\eta)J(\xi,\eta)d\xi d\eta\right\} \\
&-n_i(y^+)\sum_{e=1}^{ne2}\left\{\sum_{\alpha=0}^{8}\Delta u_k^\alpha(x^\alpha)\int_{\Gamma_e^+}T_{ijk}^*(x(\xi,\eta),y^+)N_\alpha(\xi,\eta)J(\xi,\eta)d\xi d\eta\right\} \qquad y^+\in\Gamma^+
\end{aligned} \tag{19}$$

where *ne1* denotes the total number of elements on the uncracked surfaces and *ne2* represents the total number of elements on the upper crack surfaces. x^α represents the nodes of each element, and x is the inner field points of each element. $J(\xi,\eta)$ is the Jacobian. For 9DQLE, $N_\alpha(\xi,\eta)=\phi_{Coll}^\alpha$ while for the crack-tip elements, $N_\alpha(\xi,\eta)=M^\alpha$.

when *y* passes through all the collocation nodes, Eq. (18) and Eq. (19) give a system of linear equations, which can be expressed in a matrix form as:

$$\mathbf{Hu}=\mathbf{Gt} \tag{20}$$

where matrix $\mathbf{H}$ contains integrals involving T_{ijk}^{*}, and matrix $\mathbf{G}$ contains integrals involving U_{ijk}^{*}. Vectors $\mathbf{u}$ and $\mathbf{t}$ consist of all nodal displacements and traction components on the boundary. Rearranging Eq. (20) according to the boundary conditions results in

$$\mathbf{Ax} = \mathbf{By} = \mathbf{f} \tag{21}$$

where $\mathbf{x}$ is the vector containing the boundary unknowns u_i, t_i and Δu_i, and $\mathbf{y}$ is the vector for known components.

4. Treatment of singular integrals

Special attention needs to be paid for the singular integrals, which arise in the TBIE. In this section, firstly an element subdivision technique is introduced. Then the classic singular subtraction method (Mi and Aliabadi, 1992; Guiggiani, 1998) in combination with the element subdivision techniques is employed for the Cauchy and Hadamard finite part integrals.

4.1 Element subdivision

The element subdivision is indispensible for treating the singular integrals in 3D cases (Zhang, 2009). In this section, we subdivide an integration element in a suitable pattern considering both element shape and the position of the source point **x** in the element. Adaptive integration based on element subdivisions is employed just as a combination for the singular subtraction method (Mi and Aliabadi, 1992; Guiggiani, 1998).

Note that although the original quadrangle has a fine shape, the four sub-triangles may have poor shapes depending on the position of **x** (the source point) (see Fig. 3(a) and Fig. 3(b)).

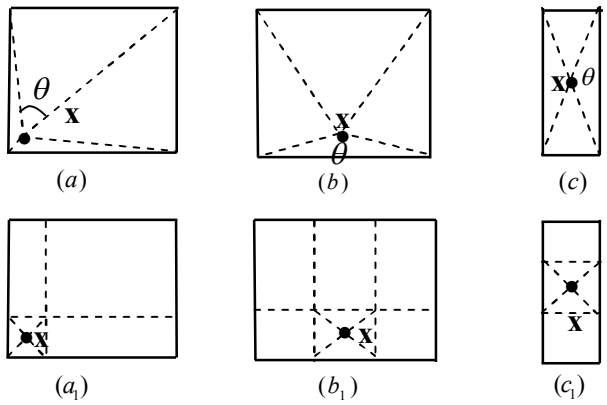

Fig. 3. Subdivisions of quadrilateral element depending on the position of the source point

Obtaining triangles with high quality seems to be more difficult by direct subdivision for irregular initial elements as shown in Fig. 3(c) even when **x** is located in the center of the quadrilateral element. If the angle θ between two lines intersected at **x** in each triangle is larger by a certain value $2\pi/3$ and even tends to π as in Fig. 3(a) – 3(b), numerical results will become less accurate.

To solve the troubles described above, we have developed an adaptive subdivision for an arbitrary quadrilateral element. The original element is divided into several triangles and additional quadrangles, which is different from these as shown in Fig. 3(a_1)-(c_1). The adaptive subdivision consists of three main steps are briefly described as follows:

First, compute the distances in the real-world-coordinate system from **x** to each edge of the element and obtain the minimum distance d.

Then, based on d, we construct a box defined in parametric system, but with square shape in the real-world-coordinate system as fine as possible, to well cover **x**.

Finally, triangles are generated in the box and additional quadrangles are created outside the box in the element.

Applying the strategy above, adaptive subdivisions for the elements in Fig. 3 with suitable patterns are shown in Fig. 3(a_1)-(c_1). For each triangle, the singular integrals are calculated by the singular subtraction method (Aliabadi et al, 1985; Mi and

Aliabadi, 1992; Guiggiani, 1998). However, for each quadrangle, nearly singular integrals will arise but not severe, which can be calculated by adaptive integration scheme based on the element subdivision technique discussed in Ref. (Zhang, 2009).

4.2 Evaluation of Cauchy and Hadamard finite part integrals

In our method, when the collocation point is located in the integration element, the element is treated as a singular element. The integrands over a singular element are highly singular and the integrals over the element are required to be treated as Cauchy or Hadamard finite part integrals. The technique which we employ in this study for evaluation of these integrals was developed by Guiggiani *et. al.* (Guiggiani 1998) who utilized a singularity subtraction technique pioneered by Aliabadi, Hall and Phemister(Aliabadi et al, 1985). In this technique, the singular part of the fundamental solution in the kernel is subtracted out and integrated analytically, or semi-analytically leaving the remaining integrand well behaved. This technique, which is based on Taylor series expansions of kernel, shape functions and the Jacobian of the transformation, has been applied to many problems. Aliabadi *et. al.* (Aliabadi *et. al.*, 1985) wrote the integral involving a product of kernel D, shape function and the Jacobian as:

$$\begin{aligned}
&\int_{-1}^{1}\int_{-1}^{1} D[P_S,Q(\xi,\eta)]N_\alpha(\xi,\eta)J(\xi,\eta)d\xi d\eta \\
&= \left\{ \begin{array}{l} \int_{-1}^{1}\int_{-1}^{1} D[P_S,Q(\xi,\eta)]N_\alpha(\xi,\eta)J(\xi,\eta)d\xi d\eta \\ -\int_{-1}^{1}\int_{-1}^{1} D^*[P_S,Q(\xi,\eta)]N_\alpha^*(\xi,\eta)J^*(\xi,\eta)d\xi d\eta \end{array} \right\} \\
&+\int_{-1}^{1}\int_{-1}^{1} D^*[P_S,Q(\xi,\eta)]N_\alpha^*(\xi,\eta)J^*(\xi,\eta)d\xi d\eta
\end{aligned} \tag{22}$$

where the approximate integrand denoted by * has the same singularity as the original integrand but of simpler form which can be integrated analytically or semi-analytically. In Eq. (22), the first integral on the right side is non-singular and can be integrated accurately by the standard numerical quadrature. Details of the singularity subtraction technique have been discussed in Refs. (Aliabadi *et. al.*, 1985; Mi and Aliabadi, 1992; Guiggiani, 1998).

It should be noted that in our work, firstly, the singular elements are subdivided into

several triangle and quadrilateral patches. Then the singularity subtraction technique is employed for the singular integrals on triangle patches while adaptive integration scheme for nearly singular integrals is applied for the regular integrals on quadrilateral patches.

5. Calculation of stress intensity factors

In our work, whenever the elasticity solution is available, the CODs which are obtained through our method can be directly used to compute the stress intensity factors. We consider a local coordinate system centered at a point O along the crack front with coordinate directions: **t** (the tangent unit vector of the front curve), **b** (the unit normal to the crack surface) and $\mathbf{n} = \mathbf{b} \times \mathbf{t} / |\mathbf{b} \times \mathbf{t}|$ point into the body as shown in Fig. 4.

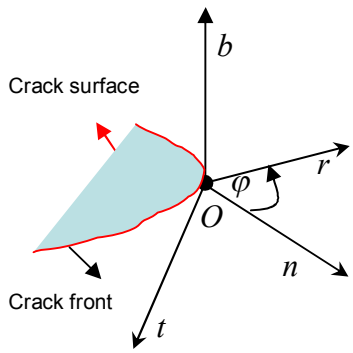

Fig. 4. Crack front local coordinate system

The stress intensity factors (Mi, 1996) can be expressed as follows:

$$K_I = \frac{E}{4(1-\mu^2)} \lim_{r \to 0} \sqrt{\frac{\pi}{2r}} \Delta u_b$$

$$K_{II} = \frac{E}{4(1-\mu^2)} \lim_{r \to 0} \sqrt{\frac{\pi}{2r}} \Delta u_n$$

$$K_{III} = \frac{E}{4(1+\mu)} \lim_{r \to 0} \sqrt{\frac{\pi}{2r}} \Delta u_t \qquad (23)$$

where $\Delta u_b = \Delta u \bullet \mathbf{b}$, $\Delta u_n = \Delta u \bullet \mathbf{n}$, $\Delta u_t = \Delta u \bullet \mathbf{t}$, μ is the Poisson's ratio and E is the Young's Modulus.

Due to the use of discontinuous elements, CODs obtained after boundary element analysis are at the collocation nodes inside the geometry on the edges of the element. As shown in Fig. 5, when one point formula is employed, stress intensity factors are evaluated by:

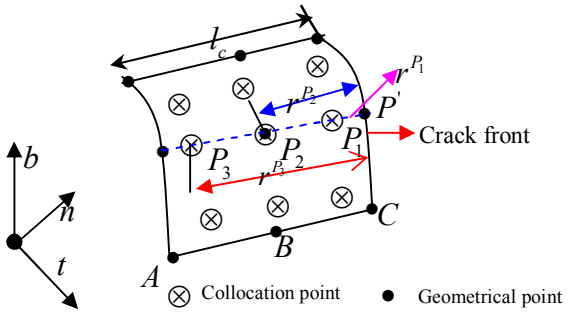

Fig. 5. A crack front element

$$K_I^{P'} = \frac{E}{4(1-\nu^2)}\sqrt{\frac{\pi}{2r}}\Delta u_b^P$$

$$K_{II}^{P'} = \frac{E}{4(1-\nu^2)}\sqrt{\frac{\pi}{2r}}\Delta u_n^P$$

$$K_{III}^{P'} = \frac{E}{4(1+\nu)}\sqrt{\frac{\pi}{2r}}\Delta u_t^P \tag{24}$$

where the CODs $\Delta\mathbf{u}^P$ are evaluated at point P (such as P_1, P_2, P_3) as shown in Fig. 5, $\Delta u_b^P, \Delta u_n^P, \Delta u_t^P$ are the projections of $\Delta\mathbf{u}^P$ on the coordinate directions of the local crack front coordinate system as shown in Fig. 4.

In our work, a modified COD extrapolation technique is used to assess the stress intensity factors. We assume that points P_1, P_2, P_3 and the crack front point P' are on the same line as illustrated in Fig. 5. The distances between P_1 and P', P_2 and P', P_3 and P' are denoted as r^{P_1}, r^{P_2}, and r^{P_3}, respectively. The stress intensity factor evaluated by the formula (24) from the relative CODs at points P_1, P_2, and P_3 are symbolized as K^{P_1}, K^{P_2}, K^{P_3}, respectively. In our work, the stress intensity factors corresponding to the point P' can be expressed by a linear extrapolation of K^{P_2} and K^{P_3}.

$$K^{P'} = \frac{r^{p_3} K^{p_2} - r^{p_2} K^{p_3}}{r^{p_3} - r^{p_2}} \tag{25}$$

6. Numerical examples

Example 1: A penny shaped crack in an infinite solid under shear

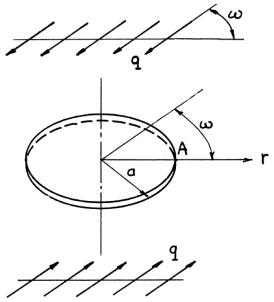

Fig. 6. A penny shaped crack in an infinite solid under shear (Tada et al, 2000)

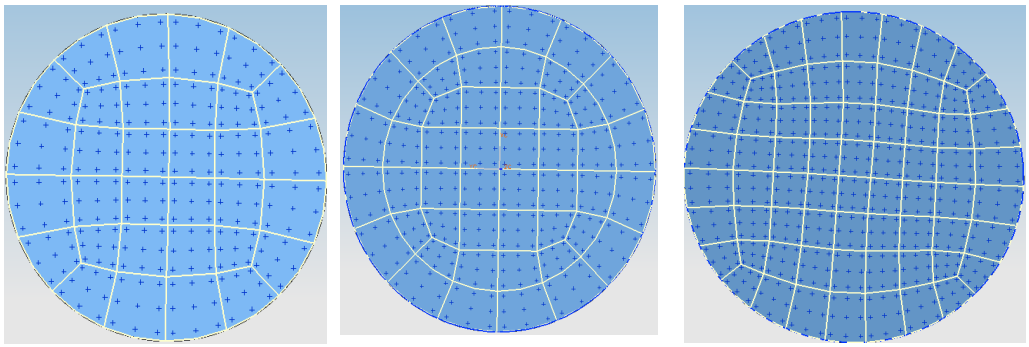

(*a*) (*b*) (*c*)

Fig. 7. Boundary element (BE) discretization of the crack model:

(a) 32 elements (b) 48 elements (c) 68 elements

As shown in Fig. 6, a penny shaped crack in an infinite solid under shear is considered. The radius (a) is 1 and the shear (q) is 1. The Young's Modulus (E) is 1 and the Poisson's ratio (v) is 0.25. Three different meshes are employed in the example and the meshes are depicted in Fig. 7. Convergence of the SIFs is also studied while the number of elements ranges from about 32 to 68. The exact SIFs for this problem are given by Tada (Tada et al, 2000) as follows:

$$K_{IA} = 0$$

$$K_{IIA} = \frac{4}{\pi(4-v)}(q\cos w)\sqrt{\pi a}$$

$$K_{IIIA} = \frac{4(1-v)}{\pi(2-v)}(q\sin w)\sqrt{\pi a} \tag{26}$$

The convergence of three kinds of SIFs is shown in Fig. 8. In Fig. 8, it can be noted that the solutions of all the meshes are indistinguishable from the exact solutions. The exact solutions and the solutions of all the meshes are seen to overlap along the crack front. The largest error for the SIFs using our method is about 1 percent compared with exact solutions. High accuracy can be achieved by our method, even though the mesh (a) is coarse.

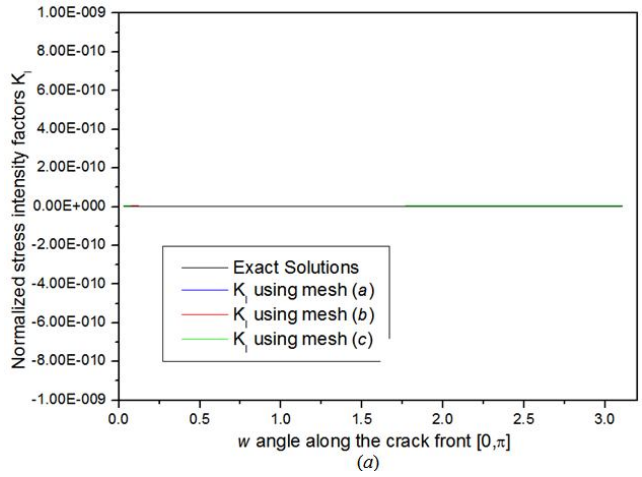

(*a*)

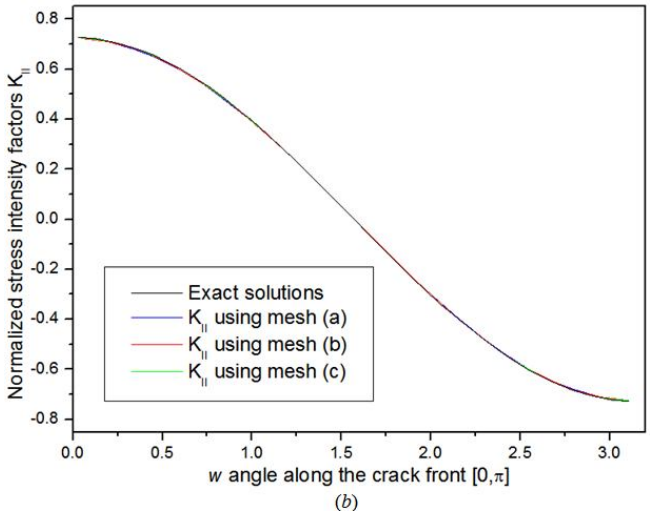

(*b*)

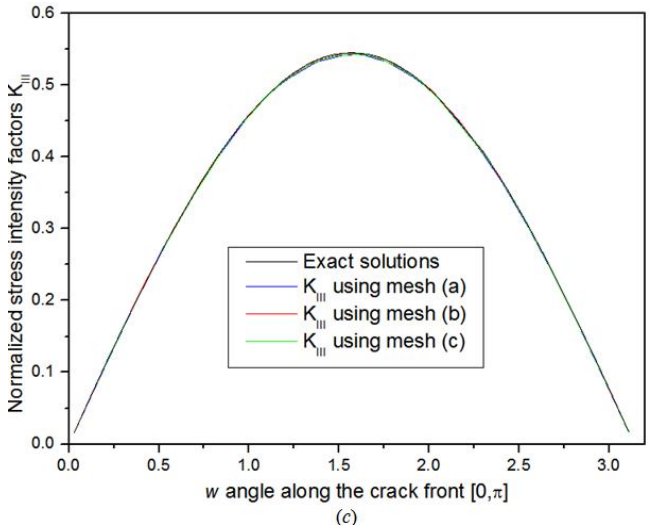

(*c*)

Fig. 8. Normalized SIFs along the front of the penny shaped crack: (a) model I SIFs (b) model II SIFs (c) model III SIFs

Example 2: A singular edge crack

In this example, we concern a rectangular edge crack bar specimen of thickness *t*, width *w* and total height *2h*, with a crack length *a* through the thickness as shown in Fig. 9. The ends of specimen are subjected to a uniform uniaxial tensile stress σ in the *y*-direction, perpendicular to the crack. The BE mesh is shown in Fig. 10 and the normalized stress intensity factors, (i.e. $K_I / \sigma\sqrt{\pi a}$) for *t/a=2*, *w/a=3*, *h/a=1.75* or *h/a=6* along the crack front are illustrated in Fig. 11 together with the results obtained by Raju & Newman (Raju and Newman, 1977) using the finite element method. The SIF at the center of the bar computed by our method is 2.8254 when *h/a=6*. This value is in good agreement with that in Ref. (Murakami, 2001) (In that paper, the SIF is 2.827). The difference between the two values is within 0.06 percent and in Ref. (Raju and Newman, 1977), the SIF is 2.776. When *h/a=1.75*, the SIF is 2.83575 by our method. The value obtained by our method is within 0.4 percent within that of Murakami's method and the SIF is 2.787 in Ref. (Raju and Newman, 1977). It should be noted that compared with Raju and Newman's method, the results for the stress intensity factor at the center of the bar obtained by our method are closer to the Murakami's results. When $z/w \approx 0.48$, the value of our method is 2.641 for *h/a=6* and the value of our method is 2.680 for *h/a=1.75*, while in Ref. (Raju and Newman,

1977), the value is 2.441 for *h/a=6* and 2.434 for *h/a=1.75*. The difference between the two values is about 8.2 percent for *h/a=6* and 10.1 percent for *h/a=1.75*. In Raju and Newman's method, the SIFs are nearly uniform over most of the thickness and are lower than the midplane value near the free surface (Raju and Newman, 1977). The same trends of SIFs can also be achieved by our method as shown in Fig.11. Furthermore, the results obtained by our method are compared with those of Mi and Aliabadi (Mi and Aliabadi, 1992). When $z/w \approx 0.48$, the value is about 2.7 for both *h/a=1.75* and *h/a=6*. The results obtained by our method are closer to these of Mi and Aliabadi's method. The largest error of the two cases is within 2.2 percent compared with Mi and Aliabadi's method (Mi and Aliabadi, 1992). Moreover, results presented in Fig. 11 show that the K_I variation along the crack front is in good agreement with the work of Mi and Aliabadi (Mi and Aliabadi, 1992). So the present results can be acceptable compared with the previous results.

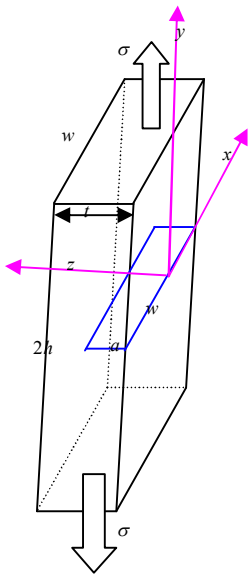

Fig. 9. Geometry model of the singular edge crack

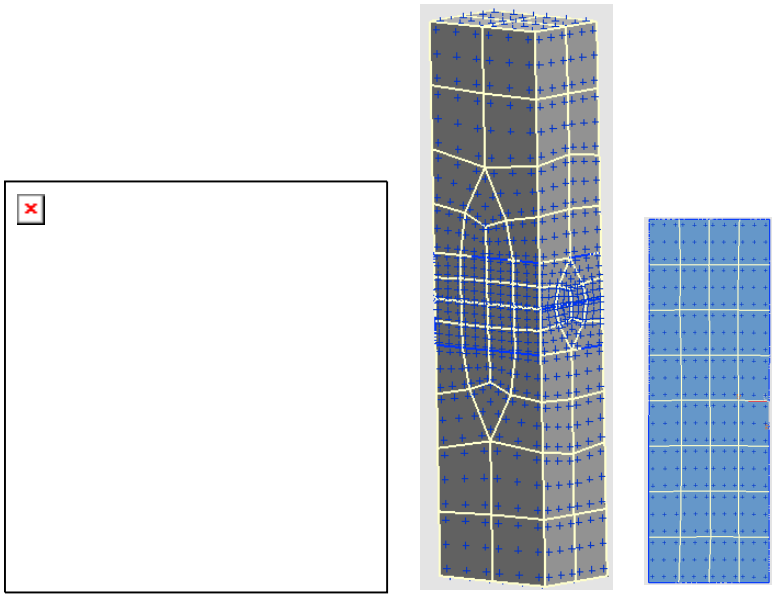

(*a*) (*b*) (*c*)

Fig. 10. A singular edge crack model

(a) BE discretization of the external boundary when *h/a=1.75*

(b) BE discretization of the external boundary when *h/a=6*

(c) BE discretization of the crack

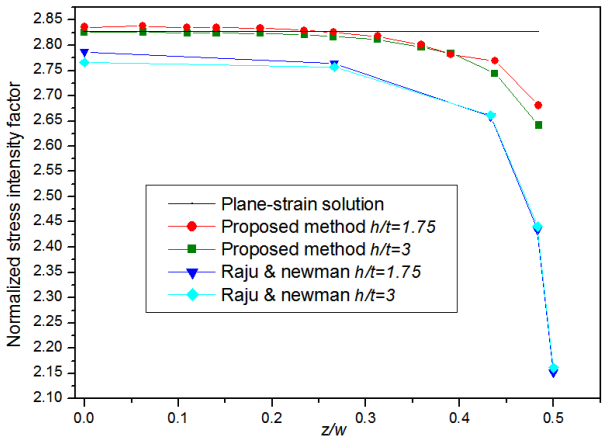

Fig. 11. Normalized SIFs along the front of the single edge crack

Example 3: *A semi-elliptical surface crack in a finite-thickness plate*

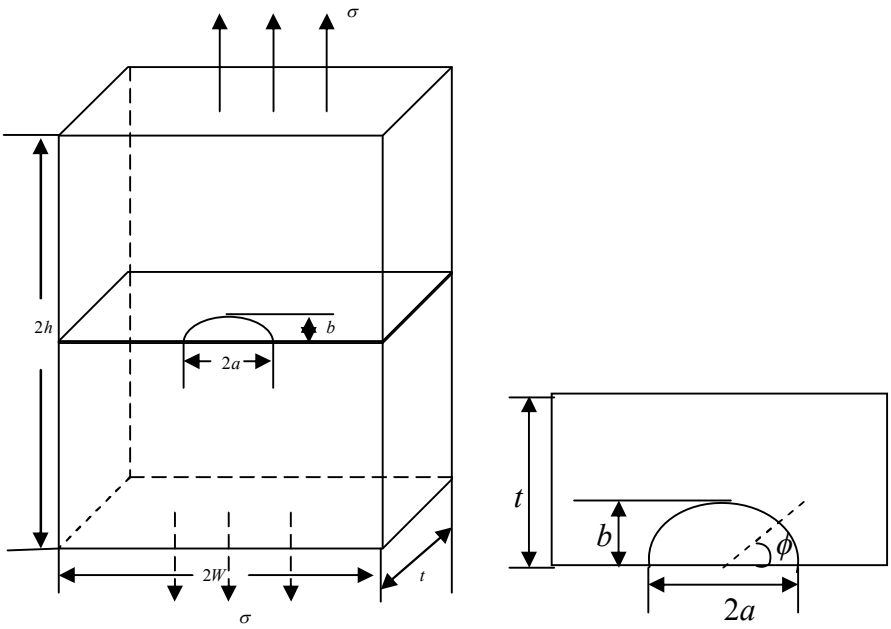

Fig. 12. A semi-elliptical surface crack in a finite-thickness plate

As shown in Fig. 12, a semi-elliptical plane crack is contained in mid-cross-section of a finite-thickness plate. The geometry of the crack and the plate are defined by: $2h=10$, $2w=10$, $t=5$, $2a=2$, $b=1$. The material properties are: the Young's Modulus E=1 and the Poisson's ratio v=0.3. The BE mesh for this problem is shown in Fig. 13 and Fig. 14. 108 discontinuous quadrilateral elements are used to discretize the plate while the crack surface is discretized with 16, 24 and 36 elements. The Model-I SIFs of the three meshes along the front of semi-elliptical surface crack are shown in Fig. 15 (the ϕ is shown in Fig. 12). Note that the mesh (a) is too coarse, the SIF has a large difference compared with that of Newman and Raju's method when $\phi=0$, whereas meshes (b) and (c) produce better results. Fig. 15 show that the results obtained by our method using mesh (c) are in very good agreement with those obtained by Newman and Raju (Raju and Newman, 1979) for the same problem using a finite element approach. In order to assess the accuracy of our method, the SIFs obtained by our method using the three meshes are also listed in Table 1, compared with Newman and Raju's method (Raju and Newman, 1979). In Table 1, the results obtained by our method using mesh (c) are generally better, and the largest error is about 1.5 percent.

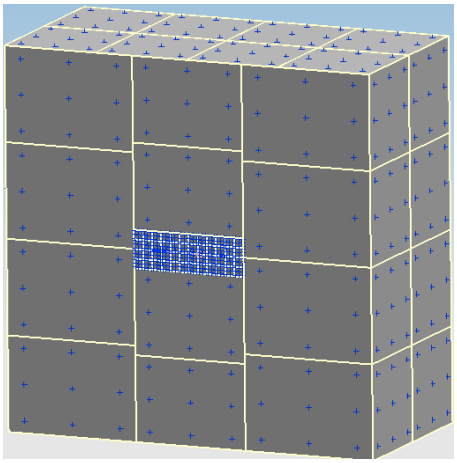

Fig. 13. BE discretization of semi-elliptical surface crack in a finite-thickness plate: BE discretization of the external boundary

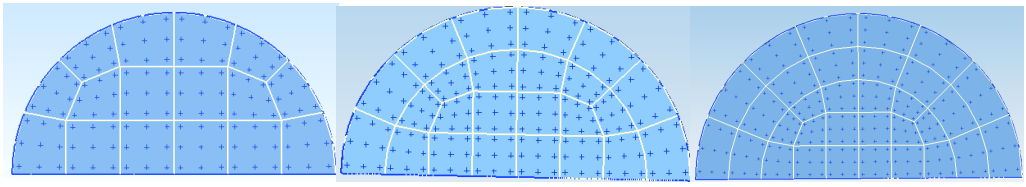

Fig. 14. BE discretization of the crack:

(a) 16 elements (b) 24elements (c) 32 elements

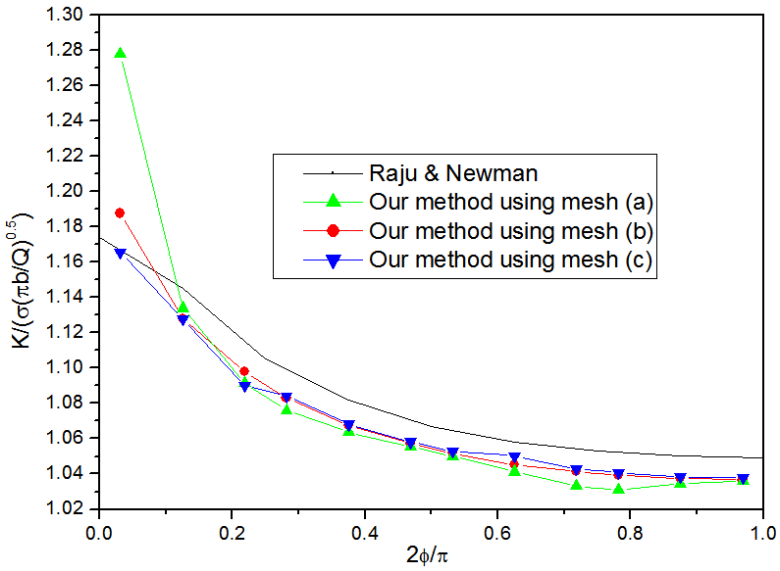

Fig. 15. Model-I SIFs along the front of semi-elliptical surface crack in a finite-thickness plate

Table 1 Comparisons between our method and *Newman and Raju's* method

$2\phi/\pi$	*Newman and Raju's method*	*our method* mesh (a)	*our method* mesh (b)	*our method* mesh (c)
0.125	1.145	1.13401	1.12814	1.1280
0.375	1.082	1.06362	1.06744	1.06823
0.625	1.058	1.04118	1.04529	1.05028
0.875	1.050	1.03423	1.03735	1.03827

7. Conclusions

This paper presented a direct TBIE formulation for three-dimensional crack problems in infinite and finite domains. This formulation was based on the TBIE. Only the TBIE was required in this formulation and this formulation had the advantage resulting in a smaller system of algebraic equation. In our method, all the surfaces of the considered structure are discretized into discontinuous quadrilateral quadratic elements, and two types of special crack-tip elements, which successfully captured the distribution of displacements in the vicinity of the crack tips, were introduced. An adaptive singular integral technique was developed to calculate the finite-part integrals over these elements. A modified COD extrapolation method was adopted for the computation of SIFs. Numerical examples of SIFs computation were given for both finite and infinite domains. The SIFs obtained by the present method were in very good agreement with previously published results. Results demonstrated the accuracy and efficiency of our method.

ACKNOWLEDGEMENT

This work was supported in part by National Science Foundation of China under grant numbers 11172098, in part by National 973 Project of China under grant number 2010CB328005 and in part by Hunan Provincial Natural Science Foundation for Creative Research Groups of China (Grant No.12JJ7001).

References

Aliabadi, M. H. (1997). Boundary element formulations in fracture mechanics. Applied Mechanics

Reviews, 50, 83.

Aliabadi, M. H., Hall, W. S., & Phemister, T. G. (1985). Taylor expansions for singular kernels in the boundary element method. International Journal for Numerical Methods in Engineering, 21(12), 2221-2236.

Blandford, G. E., Ingraffea, A. R., & Liggett, J. A. (1981). Two‐dimensional stress intensity factor computations using the boundary element method. International Journal for Numerical Methods in Engineering, 17(3), 387-404.

Cruse, T. A. (1988). Boundary element analysis in computational fracture mechanics (Vol. 1). Springer.

Crouch, S. L., & Starfield, A. M. (1983). Boundary element methods in solid mechanics: With applications in rock mechanics and geological engineering: Winchester, Massachusetts.

Chen, W. H., & Chen, T. C. (1995). An efficient dual boundary element technique for a two dimensional fracture problem with multiple cracks. International Journal for Numerical Methods in Engineering, 38(10), 1739-1756.

Cisilino, A. P., & Aliabadi, M. H. (1999). Three-dimensional boundary element analysis of fatigue crack growth in linear and non-linear fracture problems. Engineering fracture mechanics, 63(6), 713-733.

Guiggiani, M. (1998). Formulation and numerical treatment of boundary integral equations with hypersingular kernels. Singular integrals in boundary element methods, 85-124.

Lachat, J. C., & Watson, J. O. (1976). Effective numerical treatment of boundary integral equations: A formulation for three‐dimensional elastostatics. International Journal for Numerical Methods in Engineering, 10(5), 991-1005.

Mi, Y., & Aliabadi, M. H. (1992). Dual boundary element method for three-dimensional fracture mechanics analysis. Engineering Analysis with Boundary Elements, 10(2), 161-171.

Mi, Y., & Aliabadi, M. H. (1994). Discontinuous crack-tip elements: application to 3D boundary element method. International journal of fracture, 67(3), R67-R71.

Murakami, Y., & Hasebe, N. (Eds.). (2001). Stress intensity factors handbook. Elsevier Science.

Mi, Y. (1996). Three-dimensional analysis of crack growth. Computational Mechanics Publications.

Pan, E. (1997). A general boundary element analysis of 2-D linear elastic fracture mechanics. International Journal of Fracture, 88(1), 41-59.

Pan, E. (1991). Dislocation in an infinite poroelastic medium. Acta mechanica, 87(1-2), 105-115.

Pan, E., & Yuan, F. G. (2000). Boundary element analysis of three‐dimensional cracks in anisotropic solids. International Journal for Numerical Methods in Engineering, 48(2), 211-237.

Raju, I. S., & Newman, J. C. (1977). Three dimensional finite-element analysis of finite-thickness fracture specimens.

Raju, I. S., & Newman, J. C. (1979). Stress-intensity factors for a wide range of semi-elliptical surface cracks in finite-thickness plates. Engineering Fracture Mechanics, 11(4), 817-829.

Sirtori, S., Maier, G., Novati, G., & Miccoli, S. (1992). A galerkin symmetric boundary‐element method in elasticity: Formulation and implementation. International Journal for Numerical Methods in Engineering, 35(2), 255-282.

Tada, H., Paris, P. C., Irwin, G. R., & Tada, H. (2000). The stress analysis of cracks handbook (Vol. 130). New York: ASME press.

Wilde, A. J., & Aliabadi, M. H. (1999). A 3-D Dual BEM formulation for the analysis of crack growth. Computational mechanics, 23(3), 250-257.

Wang, P. B., & Yao, Z. H. (2006). Fast multipole DBEM analysis of fatigue crack growth. Computational Mechanics, 38(3), 223-233.

Zhang, J., Qin, X., Han, X., & Li, G. (2009). A boundary face method for potential problems in three dimensions. International journal for numerical methods in engineering, 80(3), 320-337.

APPENDIX A

$$M^0 = 1.254611404\xi + 1.672815209\xi^2 \text{-} 3.763834213\xi\sqrt{1+\eta}$$
$$\text{-}5.018445625\xi^2\sqrt{1+\eta} \text{-} 5.018445625\xi(1+\eta) + 3.345630416\xi^2(1+\eta)$$

$$M^1 = \text{-}1.254611404\xi + 1.672815209\xi^2 + 3.763834213\xi\sqrt{1+\eta}$$
$$\text{-}5.018445625\xi^2\sqrt{1+\eta} \text{-} 2.509222810\xi(1+\eta) + 3.345630416\xi^2(1+\eta)$$

$$M^2 = \text{-}2.143500293\xi + 2.858000394\xi^2 + 3.763834213\xi\sqrt{1+\eta}$$
$$\text{-}5.018445623\xi^2\sqrt{1+\eta} \text{-} 1.620333921\xi(1+\eta) + 2.160445229\xi^2(1+\eta)$$

$$M^3 = 2.143500292\xi + 2.858000396\xi^2 \text{-} 3.763834212\xi\sqrt{1+\eta}$$
$$\text{-}5.018445628\xi^2\sqrt{1+\eta} + 1.620333920\xi(1+\eta) + 2.160445232\xi^2(1+\eta)$$

$$M^4 = 1.881917111 + 0.5\text{e-}8\xi + \text{-}3.345630412\xi^2 \text{-} 5.645751329\sqrt{1+\eta} \text{-} 0.18\text{e-}7\xi\sqrt{1+\eta}$$
$$+10.03689123\xi^2\sqrt{1+\eta} + 3.763834218(1+\eta) + 0.13\text{e-}7\xi(1+\eta) \text{-} 6.691260818\xi^2(1+\eta)$$

$$M^5 = 2.731445032\xi \text{-} 3.641926709\xi^2 \text{-} 7.527668433\xi\sqrt{1+\eta}$$
$$+10.03689124\xi^2\sqrt{1+\eta} + 4.129556734\xi(1+\eta) \text{-} 5.506075642\xi^2(1+\eta)$$

$$M^6 = 3.215250440 + 0.3\text{e-}8\xi \text{-} 5.716000784\xi^2 \text{-} 5.645751320\sqrt{1+\eta} \text{-} 0.10\text{e-}7\xi\sqrt{1+\eta}$$
$$+10.03689124\xi^2\sqrt{1+\eta} + 2.430500880(1+\eta) + 0.6\text{e-}8\xi(1+\eta) \text{-} 4.320890456\xi^2(1+\eta)$$

$$M^7 = \text{-}2.731445031\xi \text{-} 3.641926715\xi^2 + 7.527668426\xi\sqrt{1+\eta}$$
$$+10.03689125\xi^2\sqrt{1+\eta} + \text{-}4.129556728\xi(1+\eta) + \text{-}5.506075646\xi^2(1+\eta)$$

$$M^8 = \text{-}4.097167551 + 7.283853429\xi^2 + 11.29150265\sqrt{1+\eta}$$
$$\text{-}20.07378250\xi^2\sqrt{1+\eta} \text{-} 6.194335099(1+\eta) \text{-} 0.2\text{e-}8\xi(1+\eta) + 11.01215129\xi^2(1+\eta)$$

APPENDIX B

$$M^0 = 31.87450619 + 14.16644724\xi + 14.16644717\eta - 80.06422983\sqrt{1+\xi}\sqrt{1+\eta} - 16.06324133\xi\sqrt{1+\xi}\sqrt{1+\eta} - 16.06324115\eta\sqrt{1+\xi}\sqrt{1+\eta} + 48.18972364(1+\xi)(1+\eta) - 3.79358801\xi(1+\xi)(1+\eta) - 3.79358810\eta(1+\xi)(1+\eta)$$

$$M^1 = 48.55017632 + 23.31444932\xi + 19.18489251\eta - 119.7183808\sqrt{1+\xi}\sqrt{1+\eta} - 27.44400593\xi\sqrt{1+\xi}\sqrt{1+\eta} - 16.06324078\eta\sqrt{1+\xi}\sqrt{1+\eta} + 71.16820448(1+\xi)(1+\eta) - 3.79358790\xi(1+\xi)(1+\eta) - 10.03689095\eta(1+\xi)(1+\eta)$$

$$M^2 = 63.44806842 + 26.55511681\xi + 26.55511668\eta - 159.3725312\sqrt{1+\xi}\sqrt{1+\eta} - 27.44400556\xi\sqrt{1+\xi}\sqrt{1+\eta} - 27.44400519\eta\sqrt{1+\xi}\sqrt{1+\eta} + 95.92446278(1+\xi)(1+\eta) - 10.03689065\xi(1+\xi)(1+\eta) - 10.03689086\eta(1+\xi)(1+\eta)$$

$$M^3 = 48.55017607 + 19.18489251\xi + 23.31444911\eta - 119.7183802\sqrt{1+\xi}\sqrt{1+\eta} - 16.06324097\xi\sqrt{1+\xi}\sqrt{1+\eta} - 27.44400554\eta\sqrt{1+\xi}\sqrt{1+\eta} + 71.16820413(1+\xi)(1+\eta) - 10.03689076\xi(1+\xi)(1+\eta) - 3.79358802\eta(1+\xi)(1+\eta)$$

$$M^4 = -67.6957080 - 67.6957080\xi - 29.58750589\eta + 170.0419981\sqrt{1+\xi}\sqrt{1+\eta} + 34.97167356\xi\sqrt{1+\xi}\sqrt{1+\eta} + 32.12648266\eta\sqrt{1+\xi}\sqrt{1+\eta} - 102.3462901(1+\xi)(1+\eta) + 7.58717619\xi(1+\xi)(1+\eta) + 10.03689064\eta(1+\xi)(1+\eta)$$

$$M^5 = -99.2692723 - 47.43906644\xi - 38.65678635\eta + 249.3503046\sqrt{1+\xi}\sqrt{1+\eta} + 54.88801273\xi\sqrt{1+\xi}\sqrt{1+\eta} + 34.97167358\eta\sqrt{1+\xi}\sqrt{1+\eta} - 150.0810323(1+\xi)(1+\eta) + 10.03689065\xi(1+\xi)(1+\eta) + 20.07378216\eta(1+\xi)(1+\eta)$$

$$M^6 = -99.2692714 - 38.65678600\xi - 47.43906602\eta + 249.3503027\sqrt{1+\xi}\sqrt{1+\eta} + 34.97167346\xi\sqrt{1+\xi}\sqrt{1+\eta} + 54.88801221\eta\sqrt{1+\xi}\sqrt{1+\eta} - 150.0810313(1+\xi)(1+\eta) + 20.07378195\xi(1+\xi)(1+\eta) + 10.03689071\eta(1+\xi)(1+\eta)$$

$$M^7 = -67.6957080 - 29.58750589\xi - 30.39767274\eta + 170.0419981\sqrt{1+\xi}\sqrt{1+\eta} + 32.12648266\xi\sqrt{1+\xi}\sqrt{1+\eta} + 34.97167356\eta\sqrt{1+\xi}\sqrt{1+\eta} - 102.3462901(1+\xi)(1+\eta) + 10.03689064\xi(1+\xi)(1+\eta) + 7.58717619\eta(1+\xi)(1+\eta)$$

$$M^8 = 142.5070281 + 62.86012379\xi + 62.86012350\eta - 359.9110701\sqrt{1+\xi}\sqrt{1+\eta} - 69.94334743\xi\sqrt{1+\xi}\sqrt{1+\eta} - 69.94334662\eta\sqrt{1+\xi}\sqrt{1+\eta} + 218.4040420(1+\xi)(1+\eta) - 20.07378115\xi(1+\xi)(1+\eta) - 20.07378159\eta(1+\xi)(1+\eta)$$